$\pi^+ + {}^{12}C$ elastic scattering between 18 and 44 MeV

V. Yu. Alexakhin, S. I. Gogolev, M. Kh. Khankhasayev, Zh. B. Kurmanov, K. O. Oganesyan, and E. A. Pasyuk
Joint Institute for Nuclear Research, Dubna, Moscow region, 141980 Russia

C. L. Morris, J. M. O'Donnell,* and M. W. Rawool-Sullivan
Los Alamos National Laboratory, Los Alamos, New Mexico 87545

M. K. Jones†
Rutgers University, Piscataway, New Jersey 08855

F. F. Guber and A. I. Reshetin
Institute for Nuclear Research, Troitsk, Moscow region, 117312 Russia
(Received 4 November 1997)

Differential cross sections for $\pi^+ + {}^{12}C$ elastic scattering in the energy range of 18–44 MeV for six scattering angles have been measured with an increment in the incident energy of 2 MeV. The measured cross sections are compared to calculations within the framework of a unitary scattering theory of the pion-nucleus interaction. It is shown that the excitation function at angles around 90° is dominated by the *D* wave of the pion-nucleus interaction. [S0556-2813(98)05605-2]

PACS number(s): 25.80.Dj, 25.80.Hp, 24.10.−i

I. INTRODUCTION

At energies near the (3,3) resonance pions primarily probe the nuclear surface because of the strong pion-nucleon interaction and the consequent short mean free path. At lower energies the pion mean free path in the nucleus becomes longer (~ 5 fm at $T_\pi = 50$ MeV rather than ~ 0.5 fm at $T_\pi = 180$ MeV), and information about the nuclear interior can be obtained. At pion energies below 50 MeV the available experimental data are limited to only a few experiments and do not give a complete picture of the behavior of the cross section.

In this paper new data in the energy range between 18 and 44 MeV are reported. These data together with data from previous measurements [1–9] give a rather complete description of the energy dependence of the cross section for positive pion elastic scattering from carbon in this energy region.

II. EXPERIMENT

The experiment was performed at the Low Energy Pion channel (LEP) of the Clinton P. Anderson Meson Physics Facility (LAMPF). The main goal of the experiment was to study the energy dependence of pion absorption on deuterium [10]. However, by using a single hit trigger and a CD_2 target, additional data for $\pi^+ {}^{12}C$ elastic scattering were obtained at π^+ energies of 21, 23, 25, 27, 29, 31, 33, 35, 37, 39, 41, and 45 MeV. The momentum resolution of the pion beam was varied between $\Delta p/p = 1\%$ at 45 MeV and 4% at 21 MeV.

A large solid angle detector, the LAMPF BGO-ball, was used to detect the reaction products for this study. Detailed information on the BGO-ball can be found in Refs. [10,11]. A rectangular array of nine CsI scintillators, DA1–DA9, with a 10-mm-thick upstream plastic scintillator S2, downstream of the BGO-ball was used for beam composition determination and normalization.

The target was composed of CD_2 with a cross sectional area of 1×1 cm^2 and an areal density of 0.469 g/cm^2. It was attached to a thin paper tube and placed in the center of the BGO-ball. The supporting tube was aligned along the beam axis. The diameter of the tube was large enough to keep its walls out of the beam. A thin 0.25-mm-thick plastic scintillator S1, with a cross section of 6×6 mm^2 was placed immediately upstream from the target. A coincidence between this scintillator and at least one detector of the BGO-ball formed the event trigger. A coincidence of the beam scintillator S1 with the central detector DA5 of downstream CsI array formed a beam trigger. One of every one thousand of the beam events was read out and analyzed for pion fraction determination and normalization.

The detectors of the BGO-ball were of pentagonal and hexagonal shape, tightly packed to form a truncated icosahedron of 32 sides. The detectors were distributed at an inner radius of 6.1 cm from the center of the array to the center of each crystal face, and were arranged in six rings centered at laboratory scattering angles of $\theta = 37°$, 63°, 79°, 102°, 116°, 142°. The time resolution of the detectors of about 1 ns was sufficient to eliminate the accidental coincidence of particles from different beam bursts arising from the LAMPF beam 5-ns structure. The array covered a total solid angle of $30/32 \times 4\pi$ sr. Each detector consisted of a 3-mm-thick NE102 plastic scintillator optically coupled to the front of a 5.6-cm-thick bismuth germanate (BGO) scintillator and covered a solid angle about 0.39 sr. Both scintillators were viewed by a single photomultiplier. Since the decay constant

*Present address: University of Minnesota, Minneapolis, MN 55455

†Present address: Department of Physics, College of William and Mary, Williamsburg, VA.

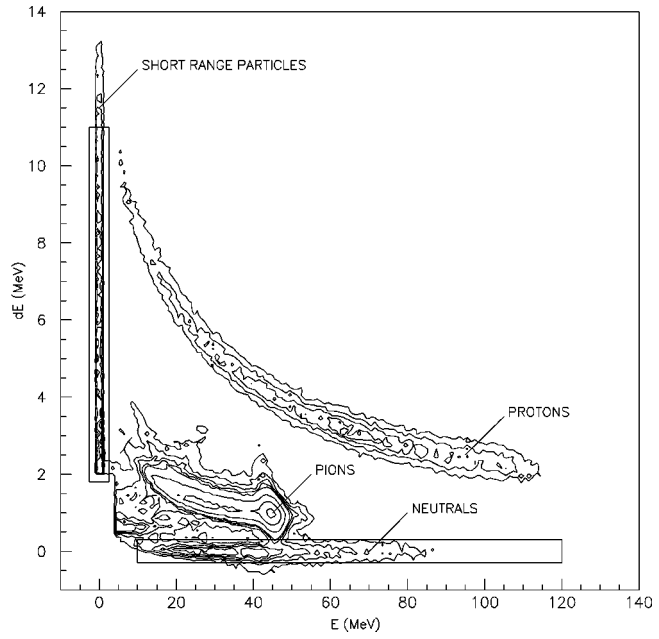

FIG. 1. Contour plot of two-dimensional distribution of ΔE (in plastic) and E (in BGO) obtained from BGO-ball phoswiches. Regions corresponding to different particle types are labeled on the plot.

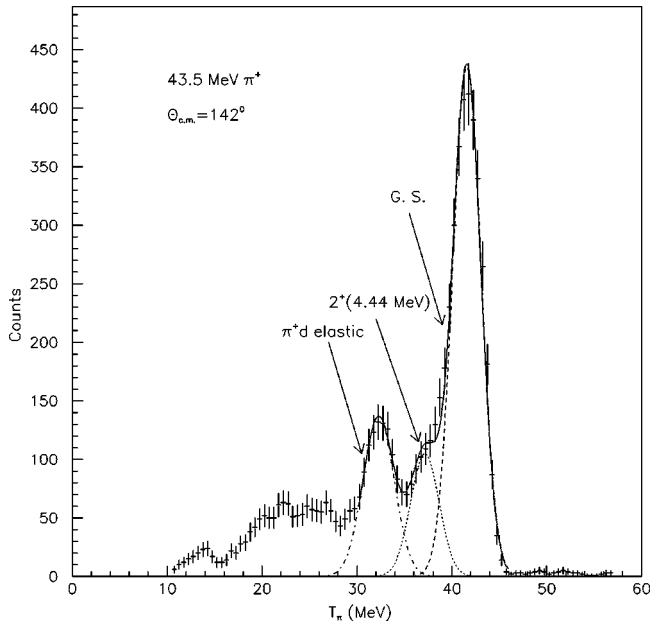

FIG. 2. A scattered π^+ spectrum for $T_\pi = 43.5$ MeV and $\theta_{\text{c.m.}} = 142°$. Dashed, dotted, and dash-dotted lines represent Gaussian fit results for ground state, 2^+ state, and $\pi^+ d$ elastic peak, respectively. The solid line is the sum of these three Gaussians.

of the BGO scintillator is much longer than that of the plastic scintillator (250 ns vs 1.5 ns), the anode signal was time sliced to provide both ΔE (fast) and E (slow) signals for charged particle identification (pions, protons, deuterons, etc.), and for identification of neutrons and γ rays. The ΔE and E signals were separated using

$$\Delta E = (\Delta E_{\text{mix}} - E_{\text{mix}} \cdot R1_{\text{mix}} - \Delta E_{\text{offset}}) \cdot G_{\Delta E}, \tag{1}$$

$$E = (E_{\text{mix}} - \Delta E_{\text{mix}} \cdot R2_{\text{mix}} - E_{\text{offset}}) \cdot G_E, \tag{2}$$

where ΔE_{mix} is a charge integrated over short (50 ns) gate, E_{mix} is a charge integrated over long (250 ns) gate, G_E and $G_{\Delta E}$ are calibration coefficients, $R1_{\text{mix}}$ and $R2_{\text{mix}}$ are a fraction of a slow component in a ΔE_{mix} signal and a fast component in a E_{mix} signal, respectively. The parameters ΔE_{offset} and E_{offset} determine the zeros of ΔE and E scales. The mixing parameters and offsets were obtained by using signals from neutral particles which have no fast component and particles stopped in plastic which have no slow component. The parameter $G_{\Delta E}$ was set to give the correct energy deposited in the plastic scintillator for protons with kinetic energies above 50 MeV where the light output from the plastic scintillator is approximately a linear function of the deposited energy [12]. The energy calibration of the BGO crystals was obtained by using the elastic peak from $\pi^+ + {}^{12}\text{C}$ scattering. An alternate calibration using the $\pi^+ d \to pp$ reaction gives similar results. Adjustments of ΔE and E gains as well as mixing parameters and offsets were performed continuously during on-line and off-line analysis because of the temperature dependence of BGO scintillator light output and the decay constant [13]. An example of the two-dimensional spectrum $\Delta E - E$ is shown in Fig. 1. A coincidence between the target detector S1 and at least one BGO crystal in anticoincidence with DA5 was used as an event trigger.

The pion flux was kept below $10^4 \pi$/s to limit pile-up in the BGO-ball detectors and to allow the beam particles to be directly counted. Pulse height and timing information from the S1, S2, and DA5 detectors was used to determine the pion fractions. A cut was placed on the time between S1 and S2 to eliminate accidental coincidence between particles from different beam bursts. Another cut was applied to a two-dimensional $\Delta E - E$ distribution (pulse height from S2 and DA5) to eliminate positron events. Modified Moyal functions [14] were used to describe the shape of the energy loss distribution in S2:

$$F(E) = P_1 e^{[-P_3(E-P_2) - e^{-P_4(E-P_2)}]}, \tag{3}$$

where E is the energy loss in S2 and $P_1 - P_4$ are adjusted parameters. The spectrum was fitted with a sum of two such functions, one for pions, and the other for muons. The fitted pion distribution was integrated to obtain the pion fraction. For the two lowest energies (21 and 23 MeV) some pions lost all of their energy in S2 and did not hit DA5. The corresponding pion peak has a different, more complicated shape. In this case only the muon peak was fitted and pion fraction was determined as the result of a subtraction of muon fraction from the integral number of beam particles.

A Monte Carlo simulation of beam particles passing through the setup using the GEANT code [15] has been performed. Corrections for energy loss, straggling, multiple scattering and decay were calculated from this simulation. The resulting correction to the normalization is 7% for the highest beam energy and 44% for the lowest one. For beam energies of 21 and 23 MeV this correction accounts for pions, which passed through the target but did not hit DA5

TABLE I. Differential cross sections. Overall systematic uncertainty of 5% is not included in total error.

T_π [a] (MeV)	$\theta_{\text{c.m.}}$ (deg)	$d\sigma/d\Omega_{\text{c.m.}}$ (mb/sr)	Statistical error	Normalization [b] error (%)	Total [c] error
18.8	37	18.28	1.13	5.0	1.46
	65	3.79	0.36		0.41
	83	3.93	0.42		0.46
	103	5.19	0.56		0.62
	118	7.39	0.76		0.84
	142	8.02	0.64		0.75
20.9	37	13.27	0.94	4.2	1.10
	65	3.89	0.37		0.41
	83	4.19	0.23		0.29
	103	5.14	0.43		0.48
	118	6.48	0.39		0.48
	142	7.78	0.38		0.50
22.9	37	9.44	0.60	4.5	0.73
	65	4.39	0.35		0.40
	83	4.60	0.47		0.51
	103	5.48	0.29		0.38
	118	7.85	0.38		0.52
	142	8.54	0.36		0.52
25.0	37	11.23	0.76	4.1	0.89
	65	4.08	0.36		0.40
	83	4.28	0.37		0.41
	103	6.00	0.34		0.42
	118	8.45	0.33		0.48
	142	8.99	0.37		0.53
27.1	37	7.88	0.58	3.7	0.65
	65	3.14	0.29		0.32
	83	4.13	0.28		0.32
	103	6.37	0.32		0.39
	118	8.67	0.37		0.49
	142	7.87	0.36		0.46
29.2	37	6.59	0.66	3.6	0.70
	65	3.28	0.31		0.33
	83	3.96	0.34		0.37
	103	6.87	0.34		0.42
	118	8.06	0.42		0.51
	142	8.40	0.34		0.45
31.2	37	6.77	0.71	3.5	0.75
	65	3.26	0.26		0.29
	83	3.77	0.25		0.29
	103	6.32	0.38		0.44
	118	7.64	0.35		0.44
	142	8.66	0.43		0.52
33.3	37	4.94	0.53	4.2	0.56
	65	3.20	0.30		0.33
	83	3.40	0.25		0.28
	103	5.62	0.30		0.37
	118	7.57	0.35		0.46
	142	7.61	0.36		0.46
35.4	37	4.23	0.38	4.0	0.41
	65	2.44	0.19		0.21
	83	3.19	0.20		0.23
	103	5.02	0.26		0.33
	118	6.64	0.24		0.36
	142	7.13	0.27		0.39

TABLE I. (*Continued*).

T_π [a] (MeV)	$\theta_{\text{c.m.}}$ (deg)	$d\sigma/d\Omega_{\text{c.m.}}$ (mb/sr)	Statistical error	Normalization [b] error (%)	Total [c] error
37.4	37	4.68	0.40	4.9	0.46
	65	3.02	0.37		0.39
	83	4.00	0.24		0.31
	103	6.75	0.32		0.45
	118	8.51	0.38		0.56
	142	8.88	0.40		0.59
39.5	37	5.05	0.47	3.4	0.50
	65	3.13	0.27		0.29
	83	4.47	0.26		0.30
	103	6.98	0.31		0.39
	118	8.21	0.35		0.44
	142	8.02	0.38		0.46
43.5	37	5.71	0.49	3.8	0.53
	65	3.37	0.27		0.30
	83	4.53	0.21		0.27
	103	7.39	0.34		0.44
	118	8.22	0.29		0.42
	142	7.63	0.26		0.37

[a]Energy in the center of target.

[b]Same value for all six angles at given energy.

[c]Total error is the statistical and normalization error summed in quadrature.

and were lost from the beam trigger. This simulation also was used for calculating the pion energy at the center of the target.

The cross sections were also corrected for counting rate losses due to dead time. A typical value of the dead time was 5%. The uncertainty in the normalization is 3–5% and it is mainly due to fitting error, the statistical error is less than 1%.

Most of the pions stopped in a BGO scintillator decay via $\pi^+ \rightarrow \mu^+ + \nu_\mu$ and muons subsequently by $\mu^+ \rightarrow e^+ + \nu_e + \tilde{\nu}_\mu$ with lifetimes of 26 and 2.2 μs, respectively. Energy deposited in the BGO by the decay products during integration time (250 ns) will be detected. Within that time almost all pions decay, resulting in a muon which deposits 4.1 MeV kinetic energy in the crystal. This additional energy does not affect the energy resolution. However, the positron from muon decay, which has a kinetic energy between 0 and 53 MeV, produces the high-energy tail which can be observed in Fig. 2. This tail contains about 9% of all stopped pion events.

The largest background in this experiment is due to nontarget-related events originating from beam pion decay near the S1 detector where the decay muon triggers the detection system. For the 21–45 MeV pions, the decay rate of the beam is about 21–14 %/m. This background is most important for the first ring of the BGO-ball located at small scattering angle since the μ^+'s are confined in a narrow cone with an opening angle of $\theta \leqslant 30°$ for our pion energies. Another source of background is the beam particles scattering on the beam scintillator S1 and its surroundings. Background measurements made with only the target removed were subtracted from the measurements with the target in place.

After background subtraction the pion spectrum was fitted with 2–3 Gaussians to separate quasielastic scattering on carbon [the excitation of the 2^+(4.44 MeV) level] and $\pi^+ d$-elastic scattering from π^{+12}C-elastic scattering. Since the resolution of the detectors was about 3.5 MeV (full width at half maximum), least-squares fitting using the known locations of the quasielastic and $\pi^+ d$-elastic peaks with respect to the π^{+12}C-elastic peak was used to extract the elastic cross sections. Using the same widths for all peaks allowed overlapping peaks to be reliably separated. Figure 2 shows the pion spectrum in the sixth ring (142°) of the BGO-ball. The differential cross section at each angle was calculated taking into account the angular acceptance of the detectors, pion decay between the target and the detector, pion nuclear reactions in the detector, $\pi \rightarrow \mu \rightarrow e$ decay in the detector, and the scattering of the pion out of the detector before it is stopped.

III. RESULTS AND DISCUSSION

The measured differential cross sections are presented in Table I and in Fig. 3. The statistical errors include contribution from peak fitting. The total error was obtained by adding the statistical and normalization errors in quadrature. An overall systematic uncertainty of about 5% in the efficiency calculation is not included in the total error. This affects the global normalization of all measured differential cross sections but does not change their relative values. A comparison of cross sections for the $\pi^+ d \rightarrow pp$ reaction, measured in the same experiment, with the partial wave analysis [10] demonstrates that our estimate of systematic uncertainties is reasonable.

We compared the measured cross sections with calculations within the framework of a unitary scattering theory

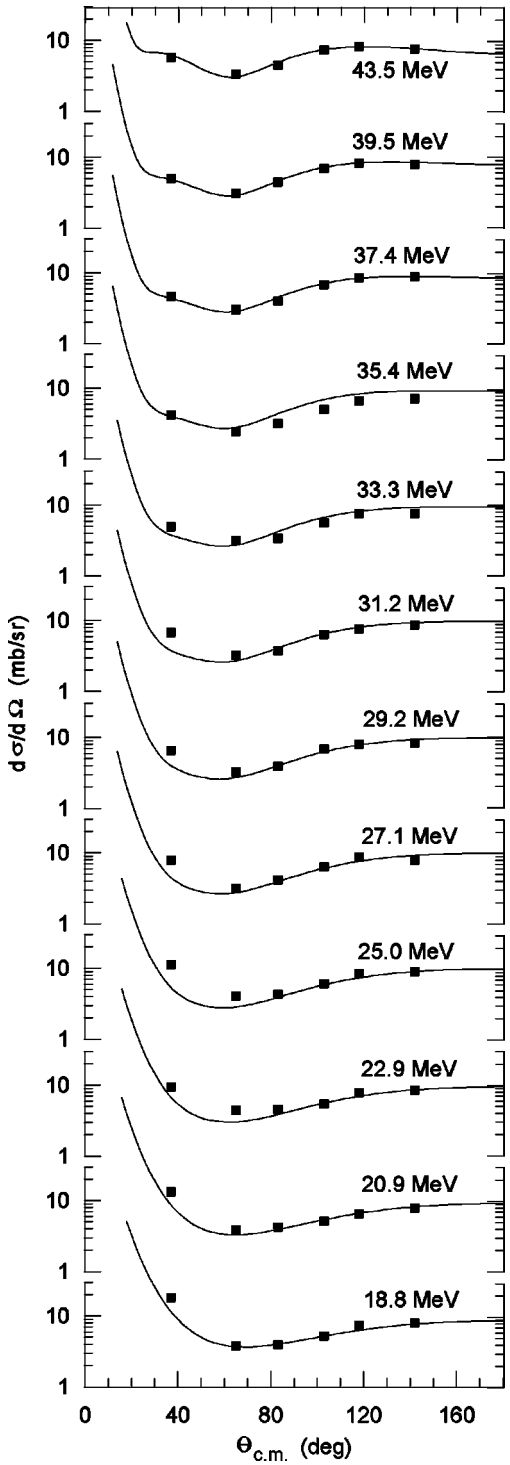

FIG. 3. Differential cross sections. Black squares are the data from this experiment. Solid lines are the UST calculations.

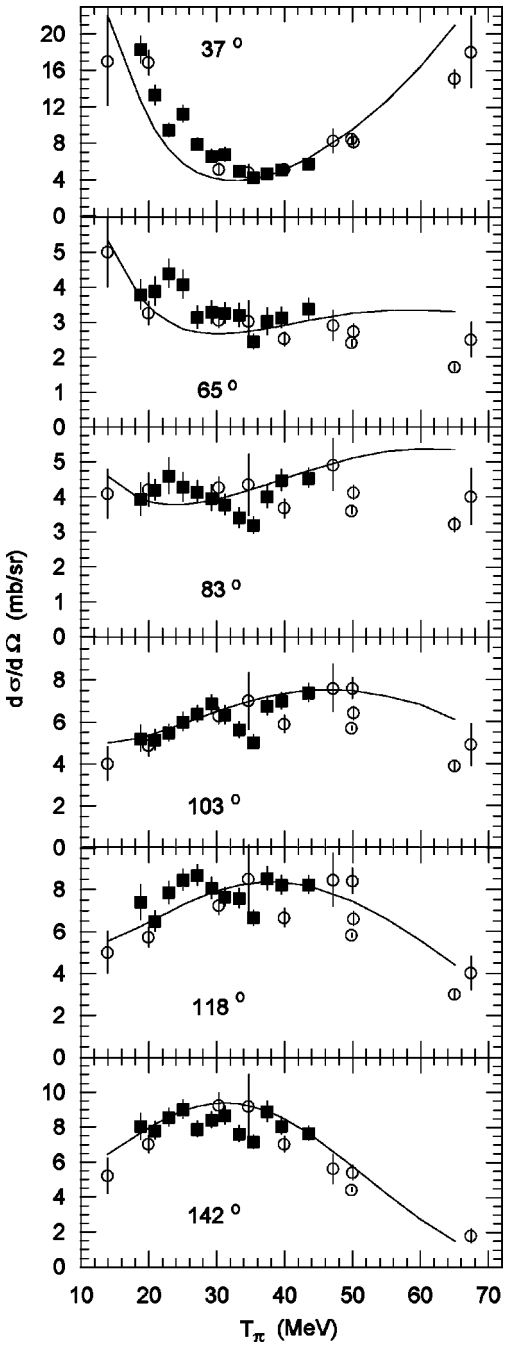

FIG. 4. Excitation functions at fixed scattering angles. Black squares are the data from this experiment. Open circles are the data from Refs. [1–9]. Solid lines are the UST calculations.

(UST) [16] of the pion-nucleus interaction. The UST approach has been specifically designed for the description of scattering of low-energy pions (below 80 MeV) by nuclei. This approach is based on the method of evolution of the system with respect to the pion-nucleon coupling constant which ensures the consistency of the theory to the unitarity condition. The latter is very important at low energies where pion-nucleus dynamics is strongly influenced by the pion absorption channel. For example, at the energies below ~ 30 MeV the reaction cross section dominated by the absorption channel, and at energies around 50 MeV one can observe a strong interference between pure potential scattering channels and the pion absorption channel. Impressive agreement between the earlier UST calculations [16] and the recently measured pion-carbon reaction and total cross sections at energies from 42 to 65 MeV has been demonstrated in Ref. [17].

The basic quantities which are calculated in the UST approach are the pion-nucleus scattering partial phase shifts

$$\delta_{\pi A}(k) = \delta^{\rm pot}_{\pi A}(k) + \delta^{\rm abs}_{\pi A}(k). \tag{4}$$

Here, $\delta^{\rm pot}$ is the part of the pion-nucleus phase shift that is

due to the multiple scattering of a pion by the nuclear nucleons, and $\delta^{\rm abs}$ is the absorption correction.

There is a multiple-scattering series [16] for a microscopic calculation of $\delta^{\rm pot}_{\pi A}$ in terms of pion-nucleon phase shifts and nuclear ground-state characteristics such as nuclear form factors and correlation functions. It has been shown in Ref. [16] that at energies below 70 MeV it is sufficient to calculate only the lowest two iterations of this series. The only free parameter of the theory is an average excitation energy parameter Δ. This parameter is introduced to take into account the excited states of the nucleus when the closure approximation is used for the calculation of the imaginary part of $\delta^{\rm pot}_{\pi A}$. Therefore, this parameter determines a threshold behavior of the inelasticity parameters

$$\text{Im } \delta^{\rm pot}_{\pi A} \sim k_{\Delta}, \tag{5}$$

where the momentum k_{Δ} is determined by the equation $E_0(k)-E_0(k_{\Delta})-\Delta=0$, $E_0(k)=\omega_{\pi}(k)+\omega_A(k)$ is the collision energy. In the nonrelativistic case, $k_{\Delta}=\sqrt{k^2-2M_{\pi A}\Delta}$, $M_{\pi A}$ is the pion-nucleus reduced mass.

As it has been shown in Ref. [16], the parameter Δ can be determined using the data on the reaction and total cross sections, and the best description of the data is provided by $\Delta=15$–25 MeV. In our calculations we use $\Delta=20$ MeV. It should be noted that the ± 5 MeV variation of the value of Δ around this value has a very weak effect on differential cross sections at energies below 50 MeV because of a dominant contribution of the pion absorption term in the formation of the imaginary part of partial phase shifts (Im $\delta=$ Im $\delta^{\rm pot}$ + Im $\delta^{\rm abs}$).

The absorption part is expressed in terms of the absorption parameters $\widetilde{B}_0$ and $\widetilde{C}_0$:

$$\delta^{\rm abs}_{\pi A}(k)=A(A-1)\frac{1+\epsilon}{1+2\epsilon/A}\hat{\rho}^2(\vec{q})[\widetilde{B}_0(k)+\widetilde{C}_0(k)(\vec{\kappa}'\cdot\vec{\kappa})], \tag{6}$$

where, $\epsilon=\omega_{\pi}(k)/2M$, ω_{π} is the pion energy, M is the mass of a nucleon, $\hat{\rho}^2(\vec{q})$ is the Fourier transform of the square of nuclear density $\rho(r)$ (normalized to unity), $\vec{q}=\vec{k}'-\vec{k}$ is the momentum transfer, and $\vec{\kappa}$ and $\vec{\kappa}'$ are the pion momenta in the $\pi-2N$ center-of-mass system. As has been shown in Ref. [16], one can neglect the energy dependence of the absorption parameters at the energies below 50 MeV, and their values are determined from the data on the strong interaction shifts and widths in the 1S- and 2P-levels of pionic atoms. The set of the absorption parameters given in Ref. [16], which provides a good description of the scattering data is

$$\widetilde{B}_0(k)=(-0.1+i0.1)\ \ \text{fm}^4=(-0.025+i0.025)m_{\pi}^{-4},$$

$$\widetilde{C}_0(k)=(-2.8+i1.0)\ \ \text{fm}^6=(-0.35+i0.13)m_{\pi}^{-6}. \tag{7}$$

Figure 3 shows the good agreement of the data for the $\pi^+ + {}^{12}$C differential cross sections measured in this experiment with the calculations within the framework of the UST approach.

The present measurements of the differential cross sections with an increment of 2 MeV make it possible to compare the data with the calculations for the excitation functions at different scattering angles: $\theta=37°$, $65°$, $83°$, $103°$, $118°$ and $142°$. Although an overall quantitative description of the data presented in Fig. 4 is satisfactory, one can see an obvious discrepancy at the angles around 90°. The measured data hint at some oscillating structure at angles $\theta=65°$, $83°$ and $103°$ for the energies from 25 to 35 MeV, while the calculated excitation functions vary rather smoothly.

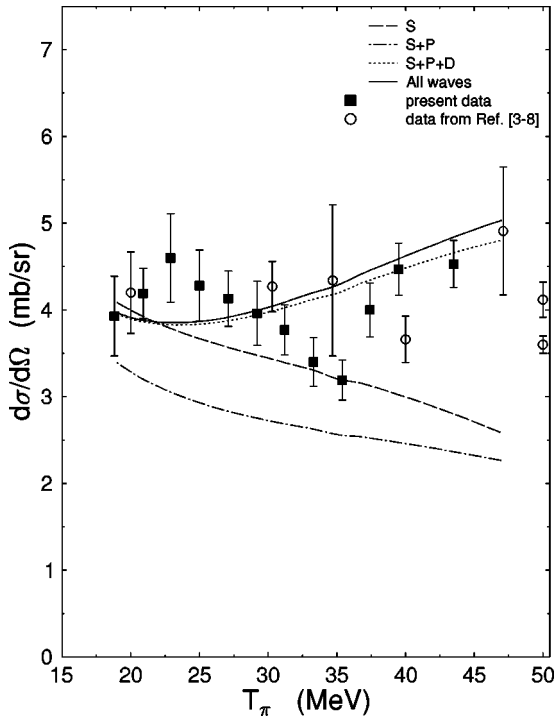

FIG. 5. Excitation function at $\theta_{\rm c.m.}=83°$. Black squares are the data from this experiment. Open circles are the data from Refs. [3–9] for the angles close to 83°. The solid line is the UST calculations including all partial waves, the dashed line is S-wave only, the dash-dotted line is $S+P$ waves, and the dotted line is $S+P+D$ waves.

Figure 5 shows the calculated contributions from the different partial waves to the excitation function at $\theta=83°$. At angles close to 90° the excitation function is dominated by S and D waves, and the D wave contribution starts to determine the shape of the excitation function at the energies above 20 MeV. Therefore, the data at angles close to 90° may provide information on the pion-nucleus D-wave interaction. Since the calculated partial waves (S, P, and D) show smooth energy dependence it is difficult to understand the irregular behavior of the data in this angular region. Since the previous data from Refs. [3,6,7] are not of sufficient precision to support or rule out this suggestion, more data are needed before a detailed discussion of a possible explanation of the oscillating structure in the excitation function at angles near 90° and the energy range 25–35 MeV can be given.

IV. CONCLUSIONS

We presented experimental data on the differential cross sections for $\pi^+ + {}^{12}$C elastic scattering at the pion energies

between 18 and 44 MeV. The measured cross sections were compared with the UST calculations. Agreement between measured and calculated cross section is rather good except for the angles close to 90°. It is shown that at these angles the excitation function is dominated by the *D*-wave at energies above 20 MeV, and the data at angles close to 90° provide us with the information on the pion-nucleus *D*-wave interaction at low energies.

[1] D. R. Gill, K. L. Erdman, E. W. Blackmore, W. Gyles, B. M. Barnet, C. Oram, R. R. Johnson, T. G. Masterson, and N. Grion, Phys. Rev. C **26**, 1306 (1982).

[2] R. J. Sobie, T. E. Drake, K. L. Erdman, R. R. Johnson, H. W. Roser, R. Tacik, E. W. Blackmore, D. R. Gill, S. Martin, C. A. Weidner, and T. Masterson, Phys. Rev. C **30**, 1612 (1984).

[3] K. K. Seth, D. Barlow, S. Iversen, M. Kaletka, H. Nann, D. Smith, M. Artuso, G. Burleson, G. Blanpied, G. Daw, W. J. Burger, R. P. Redwine, B. Saghai, and R. Anderson, Phys. Rev. C **41**, 2800 (1990).

[4] F. E. Obenshain, F. E. Bertrand, E. E. Gross, N. W. Hill, J. R. Wu, R. L. Burman, M. Hamm, M. J. Leitch, R. D. Edge, B. M. Preedom, M. A. Moinester, M. Blecher, and K. Gotow, Phys. Rev. C **27**, 2753 (1983).

[5] B. M. Preedom, S. H. Dam, C. W. Darden III, R. D. Edge, D. J. Malbrough, T. Marks, R. L. Burman, M. Hamm, M. A. Moinester, R. P. Redwine, M. A. Yates, F. E. Bertrand, T. P. Cleary, E. E. Gross, N. W. Hill, C. A. Ludemann, M. Blecher, K. Gotow, D. Jenkins, and F. Milder, Phys. Rev. C **23**, 1134 (1981).

[6] J. F. Amann, P. D. Barnes, K. G. Doss, S. A. Dytman, R. A. Eisenstein, J. D. Sherman, and W. R. Wharton, Phys. Rev. C **23**, 1635 (1981).

[7] M. Blecher, K. Gotow, D. Jenkins, F. Milder, F. E. Bertrand, T. P. Cleary, E. E. Gross, C. A. Ludemann, M. A. Moinester, R. L. Burman, M. Hamm, R. P. Redwine, M. Yates-Williams, S. Dam, C. W. Darden III, R. D. Edge, D. J. Malbrough, T. Marks, and B. M. Preedom, Phys. Rev. C **20**, 1884 (1979).

[8] S. A. Dytman, J. F. Amann, P. D. Barnes, J. N. Craig, K. G. R. Doss, R. A. Eisenstein, J. D. Sherman, W. R. Wharton, G. R. Burleson, S. L. Verbeck, R. J. Peterson, and H. A. Thiessen, Phys. Rev. C **19**, 971 (1979).

[9] M. Blecher, K. Gotow, R. L. Burman, M. V. Hynes, M. J. Leitch, N. S. Chant, L. Rees, P. G. Roos, F. E. Bertrand, E. E. Gross, F. E. Obenshain, T. P. Sjoreen, G. S. Blanpied, B. M. Preedom, and B. G. Ritchie, Phys. Rev. C **28**, 2033 (1983).

[10] E. A. Pasyuk, V. Yu. Alexakhin, S. I. Gogolev, K. O. Oganesyan, M. K. Jones, C. L. Morris, J. M. O'Donnell, M. W. Rawool-Sullivan, F. F. Guber, A. I. Reshetin, and I. I. Strakovsky, Phys. Rev. C **55**, 1026 (1997).

[11] R. D. Ransome, V. R. Cupps, S. Dawson, R. W. Fergerson, A. Green, C. L. Morris, J. A. McGill, J. R. Comfort, B. G. Ritchie, J. Tinsley, J. D. Zumbro, R. A. Loveman, P. C. Gugelot, D. L. Watson, and C. Fred Moore, Phys. Rev. Lett. **64**, 372 (1990); Phys. Rev. C **42**, 1500 (1990).

[12] R. L. Craun and D. L. Smith, Nucl. Instrum. Methods **80**, 239 (1970).

[13] B. Adeva *et al.*, Nucl. Instrum. Methods Phys. Res. A **289**, 35 (1990).

[14] J. E. Moyal, Philos. Mag. **46**, 263 (1955).

[15] CERN Program Library, W5013.

[16] M. Kh. Khankhasayev, Nucl. Phys. **A505**, 717 (1989).

[17] A. Saunders, S. Hoibraten, J. J. Kraushaar, B. J. Kriss, R. J. Peterson, R. A. Ristinen, J. T. Brack, G. Hofman, B. F. Gibson, and C. L. Morris, Phys. Rev. C **53**, 1745 (1996).